Localized instabilities of colloidal motion in ac electric field gradients

2008 J. Phys.: Condens. Matter 20 404212

(http://iopscience.iop.org/0953-8984/20/40/404212)

J. Phys.: Condens. Matter **20** (2008) 404212 (8pp) doi:10.1088/0953-8984/20/40/404212

Localized instabilities of colloidal motion in ac electric field gradients

Jinyu Zhao, Doris Vollmer, Hans-Jürgen Butt and Günter K Auernhammer

Max-Planck-Institut für Polymerforschung, Ackermannweg 10, D-55128 Mainz, Germany

E-mail: zhaoj@mpip-mainz.mpg.de and guenter.auernhammer@mpip-mainz.mpg.de

Received 28 April 2008, in final form 28 August 2008
Published 10 September 2008
Online at stacks.iop.org/JPhysCM/20/404212

Abstract

We investigated the behavior of suspensions of polymethylmethacrylate (PMMA) colloids in a density-matching solvent mixture of *trans*-decalin and cyclohexyl bromide in ac electric field gradients. Due to the difference of the dielectric constants of PMMA and the solvent mixture, these gradients exert a dielectrophoretic force on the colloids and drive them towards lower electric field strength. At sufficiently high field gradients, the initially homogeneous migration of colloids becomes unstable against local flows. We observed a wave-like instability of the interface between colloid-rich and colloid-poor regions. The wavelength does not depend on intrinsic time and length scales but seems to be determined by sample thickness. At higher field gradients the instability develops faster. The observed instability shows a number of similarities to the Rayleigh–Taylor instability.

(Some figures in this article are in colour only in the electronic version)

1. Introduction

Separation of colloids and cells and controlling their motion is of increasing interest in science and technology, because of the wide use of separation techniques in medicine, optics, microfluidics, food industry, etc [1–7]. One of the various separation techniques now in use [5, 7–11] is dielectrophoresis [2, 9, 12, 13]. If the dielectric constant of the colloids differs from that of the surrounding medium, an electric field polarizes the two constituents differently. In a field gradient, the material with the higher polarization is attracted by the field, leading to a net force on the colloids, i.e. the dielectrophoretic (DEP) force.

In 1958 Pohl initially pioneered research on this phenomenon, introduced the term 'dielectrophoresis' [1] and described it theoretically. In comparison to electrophoresis, dielectrophoresis acts only in field gradients. In 1966 Pohl and Hawk successfully separated living from dead cells using high-frequency non-uniform electric fields [14]. By using the frequency dependence of dielectrophoresis, Deval *et al* developed a DEP chaotic mixer to distribute colloids in a microfluidic channel [15]. DEP forces are also exerted by light fields and used to trap colloids with optical laser tweezers (see, e.g., [16]). As demonstrated by Chaikin and coworkers dielectrophoresis is a useful tool to confine colloids in an 'electric bottle' and to study growth and structure of colloidal crystals [17, 18]. Recently, Leunissen *et al* studied particle transport, phase transitions and crystallization of long-range repulsive charged colloids [19, 20].

Most of the previous work was concentrated on equilibrium behavior of colloidal systems in electric bottles. In the present study the emphasis is on the evolution of the local colloid concentration after turning on the electric field. In these early stages various types of colloid motion emerge in regions with high field gradient. We study colloid motions at electric field strength gradients of up to 7×10^9 V m^{-2} and at frequencies up to 1 MHz. Our model system consists of polymethylmethacrylate (PMMA) colloids initially homogeneously suspended in a density-matching mixture of *trans*-decalin and cyclohexyl bromide (CHB). This paper is organized as follows. In the next section we first give a brief review of the theoretical background and then describe our experimental set-up. In section 3 we present and discuss our results for the various types of colloidal motion. We show that the homogeneous migration of colloids along the field gradient becomes unstable above a critical applied field strength. Finally, in section 4 we compare the observed instability to the well-known Rayleigh–Taylor instability.

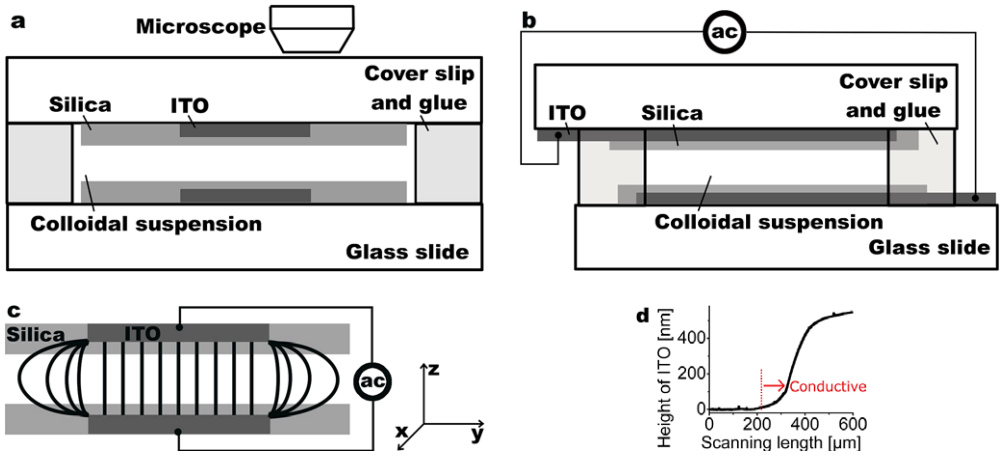

Figure 1. Sketch of our electric bottle: (a) side view of the cell, consisting of two glass slides (spaced by cover slips), ITO electrodes and a silica layer for electrical insulation, and a colloid suspension in the cell volume. The colloidal motion is observed with an optical microscope in the non-uniform electric field close to the electrode edge. (b) Side view (rotated by 90° with respect to (a)) showing the electrical connection of the electrodes. (c) Sketch of the electric field lines which are uniform between the electrodes and non-uniform close to the electrode edge. On the right the coordinate system used throughout this paper is shown (the x axis being parallel to the edges of the electrodes) if no additional comment. (d) The width of the electrode edge due to the shadow effect during sputtering.

2. Background and experimental details

2.1. Theoretical background

The DEP force on a colloid is expressed in the following way [21]:

$$\vec{F}_{\mathrm{DEP}} = 2\pi\varepsilon'_m \,\mathrm{Re}\{K^*\} r_p^3 \nabla(\vec{E}^2), \tag{1}$$

where $\vec{E}$ is the electric field strength, r_p the radius of a spherical colloid and ε'_m the real part of the complex dielectric constant of the surrounding medium. K^* is the Clausius–Mossotti factor, a function of the complex dielectric constants of the colloid (ε^*_p) and the medium (ε^*_m):

$$K^* = \frac{\varepsilon^*_p - \varepsilon^*_m}{\varepsilon^*_p + 2\varepsilon^*_m}. \tag{2}$$

The complex dielectric constants do not only include the purely dielectric parts, ε' and ε'', but also a frequency-dependent term due to the finite conductivities σ of the colloid and the surrounding medium. When neglecting dielectric losses ($\varepsilon'' = 0$) the complex dielectric constant can be written as

$$\varepsilon^* = \varepsilon' - \mathrm{j}\sigma/\omega, \tag{3}$$

with $\mathrm{j} = \sqrt{-1}$ and ω being the angular velocity of the applied field.

As can be seen from equations (1) and (2), the DEP force points towards the high (low) field region if the dielectric constant of the colloids is higher (lower) than that of the surrounding medium. Due to the conductivity term, ε^* is always a function of frequency. For sufficiently high conductivities the Clausius–Mossotti factor may change its sign as a function of frequency [9]. The conductivity term can be neglected when using solvents with low conductivity and working at high frequencies.

2.2. Materials and set-up

We use monodisperse PMMA colloids with a mean diameter of 920 nm. The PMMA colloids are sterically stabilized by poly(12-hydroxy-stearic-acid, PHS [22]), covalently bound to the colloid surface. To prevent sedimentation, we use a density-matching mixture of *trans*-decalin (Fluka) and CHB (Sigma-Aldrich) as the suspension medium (mixing ratio of approximately 22:78 in weight). The electric conductivity of both the colloids and the suspension medium is small ([23], (p 22)). In the high-frequency limit, we can simplify the Clausius–Mossotti factor as a function of the real dielectric constants:

$$K = \frac{\varepsilon'_p - \varepsilon'_m}{\varepsilon'_p + 2\varepsilon'_m}. \tag{4}$$

From the relative dielectric constant of CHB and decalin we calculate ε'_r of the solvent mixture ($\varepsilon'_r \approx 6.02$) according to [23] (p 15). Using the material parameters given in table 1 and equation (4), we find the Clausius–Mossotti factor to be

$$K = -0.126, \tag{5}$$

i.e. the DEP force points towards the lower electric field. The results reported in this paper are obtained from two representative samples, listed in table 2.

Our electric bottle follows the design described by [17, 18] and is shown schematically in figure 1. The cell consists of two glass slides (thickness 1 mm) separated by cover slips (thickness ≈150 μm). The transparent ITO electrodes are sputtered onto the glass slides and placed on the inner side of the sample cells. Near the edge the thickness of the ITO layer changes continuously from ca 500 nm to zero due to the sputtering-induced shadow effect (see figure 1(d)). The edge of the ITO seen by the microscope, i.e. the 'optical edge', coincides probably with the steepest slope. Since the ITO film is already electrically conductive at a thickness of a few tens

Table 1. The relevant parameters of the substances used: $\varepsilon_r' = \varepsilon'/\varepsilon_0$ denotes the relative dielectric constant and ε_0 the permittivity of vacuum. We determined the dynamic viscosity of CHB/decalin using a Schott Ubbelohde viscometer AVS 310. Unless noted, values are given according to the information provided by the supplier.

Material	Density (g cm^{-3})	ε_r'	Dynamic viscosity (mPa s)
PMMA	1.19	4	—
trans-decalin	0.87	2.2	3
CHB	1.324	7.9 ([23], (p 15))	2.27 ([23], (p 14))
Mixture *trans*-decalin/CHB	1.19	≈6.02	2.11

Table 2. Concentration and sample thickness.

Sample	Concentration (wt%)	Sample thickness (μm)
A	19.6	190 ± 20
B	19.6	175 ± 7

of nanometers, the 'conductive edge' differs from the optical edge by more than 100 μm. Although this conductive edge is not visible on the optical microscope images, we consider it as the real edge of the electrodes for the physics described in this paper. For electrical insulation of the electrodes from the sample, a silica layer of about 300 nm thickness is sputtered on part of the electrodes. The unprotected part of the ITO electrodes (outside the sample volume) is used for electrical connection with the ac amplifier (see figure 1(b)). Due to the relatively small separation of the electrodes, we can work with field strengths up to 1 V μm^{-1} at a maximum frequency of 1.1 MHz using a homemade amplifier. The empty cells are sealed with UV glue (Norland Products, USA), leaving only two small openings for loading the cell. Due to uncertainties in the thickness of the glue layer, sample **A** is slightly wedge-shaped with a thickness varying from 170 to 210 μm (table 2). To prevent the PMMA colloids from sticking to the silica surface, the inner side of the cell was coated with PMMA. To do so we washed the cell with a solution of PMMA in tetrahydrofuran (THF) (1 mg PMMA per ml THF, molecular weight ≈300 kg mol^{-1}) and dried the cells in the oven at 50 °C and 200 mbar over night. Finally, the cell was loaded with the PMMA colloidal suspension and sealed with UV glue.

We observed the sample using an optical microscope (Olympus BX51). The attached CCD camera is connected to a computer. We applied the commercial software Image Pro Plus (IPP) from Media Cybernetics for timed image acquisition as well as image processing and analysis. To increase image contrast we used the routines for contrast enhancement, bandpass filtering and background subtraction provided in the IPP package.

At the electrode edge the field is inhomogeneous in the y and z directions, figure 1(c). For a complete description of the dielectrophoretically induced motion both gradients should be taken into account. However, in the middle of the cell, the field gradient in the z direction vanishes. We always measured the sample thickness and adjusted the focus on the middle of the mid-plane. The depth of focus allowed observation within an approximately 30 μm thick layer. The electric field gradient in the mid-plane of the sample is simulated with the free software 'FEMM' [24]. The simulated area corresponds to the right half of the sample sketched in figure 1(c), where the origin of the y axis has been chosen to coincide with the electrode's edge. The electric field strength E in the mid-plane is plotted as a solid curve in figure 2. From this curve we get the gradient of E^2 (open squares in figure 2). Since the electric field is perpendicular to the mid-plane, ∇E^2 reduces to $\mathrm{d}E^2/\mathrm{d}y$. The scattering of the data in $\mathrm{d}E^2/\mathrm{d}y$ is due to numerical noise.

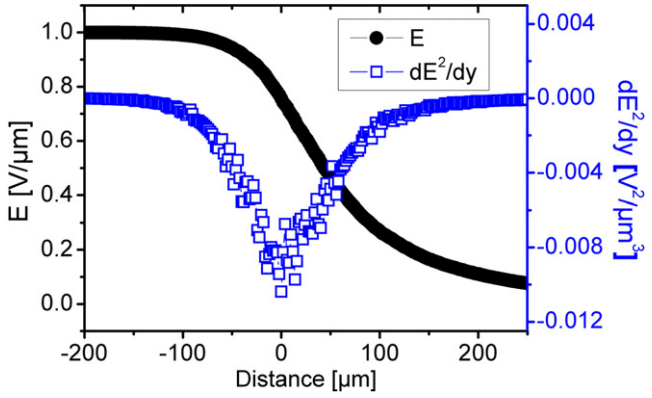

Figure 2. Numerical solution for the field strength $|E(y)|$ (solid curve) and the gradient term $\mathrm{d}E^2/\mathrm{d}y$ (open squares) in the mid-plane between the electrodes. The electrodes are situated at $y < 0$ μm. The scattering of the data in $\mathrm{d}E^2/\mathrm{d}y$ is due to numerical noise.

3. Results and discussion

3.1. Depletion zone

Before starting the experiment we allow the colloids to diffuse in order to achieve homogeneous concentration throughout the sample volume. After applying an electric field, a zone depleted of colloids appears within a few seconds at the electrode edge. Figure 3 illustrates this process from the homogeneous distribution in part (a) to the growing depletion zone in parts (b) and (c). In this figure (as throughout this paper) the electrodes are situated on the left side of the image parallel to the x axis.

Being driven by the DEP force, the colloids in lower field gradients move slower than in higher field gradients (equation (1)). This implies that the colloids on the electrode side of the maximum value of $|\mathrm{d}E^2/\mathrm{d}y|$ cannot follow the colloids close to this maximum. As a result, a depletion zone forms in the middle of the non-uniform field, parallel to the electrode edge. We are not able to precisely quantify the time-dependent colloid concentration in the depleted zone. According to our optical investigations the colloid concentration decreases to the order of 50% of the initial concentration. The depletion zone is defined as the region having a increased transmittance of at least 60% of the difference between the normal level and the brightest area. The width of the depletion zone grows with time. Due to

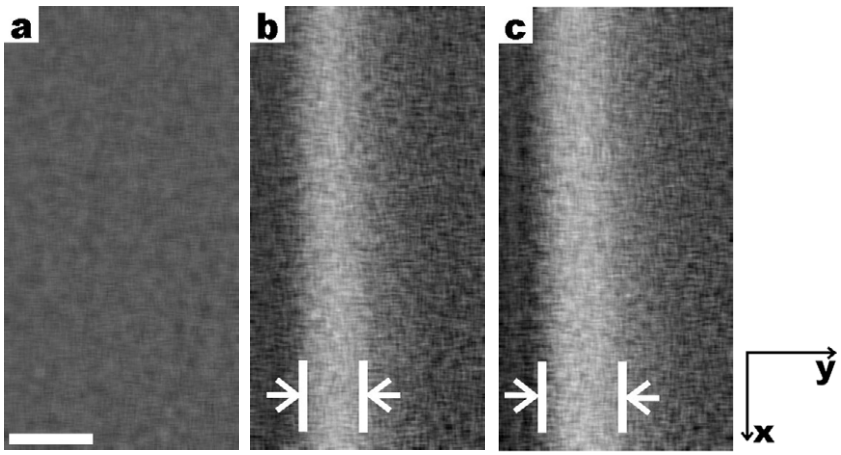

Figure 3. Evolution of the colloid concentration in the gradient region of the electric field. The left side of each image corresponds to the high and the right side to the low field region. The gray scales denotes the colloid concentration. Before turning on an electric field (0.75 V μm^{-1}, 100 kHz, sample **A**) the colloids are homogeneously distributed (a). After turning on the field a colloid-depleted zone (lighter gray) evolves, surrounded on both sides by domains with higher concentration. The width of the depleted zone is labeled with arrows in panels (b) and (c). Images (b) and (c) are taken 5 and 7 s after turning on the field, respectively. The scale bar is 100 μm.

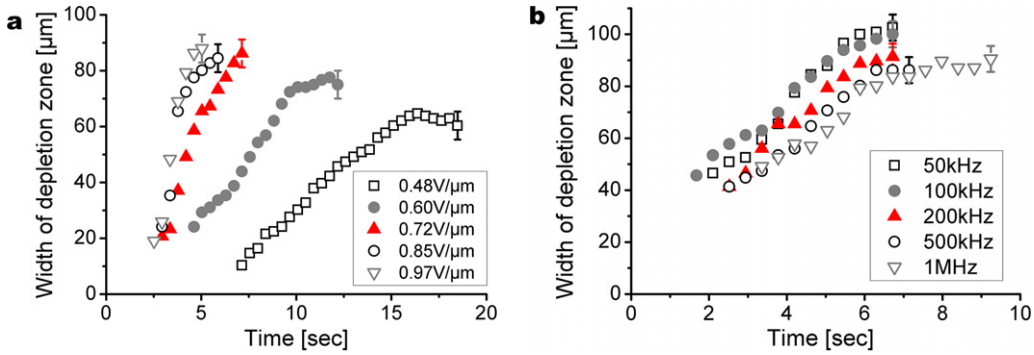

Figure 4. (a) The width of the depletion zone increases with time (various electric field strengths at a frequency of 100 kHz, sample **A**). (b) The width of the depleted zone slightly decreases for increasing frequencies at a constant electric field strength of 0.75 V μm^{-1} (sample **A**). The uncertainty of the measurements is approximately 5 μm, as indicated by the error bar of the last point of every dataset.

this formation mechanism, the edges of the depletion zone are smeared out over several micrometers. This leads to an uncertainty in the measurements of about 5 μm.

In figure 4(a) the temporal development of the depletion zone for electric field strengths ranging from about 0.5 to 1 V μm^{-1} at 100 kHz is plotted. The width of the depletion zone grows approximately linearly with time until it reaches a plateau value. This plateau coincides with a crossover to a more complex motion of the colloids. The formation of a depletion zone typically takes a few seconds, depending on the applied electric field. The higher the electric field, the faster the depletion zone forms.

To quantify the influence of the frequency of the applied field, we observed the growth of the depletion zone at a constant field strength of 0.75 V μm^{-1} for frequencies in the range of 50 kHz to 1 MHz (figure 4, right). For all frequencies, first the depletion zones grow linearly with time and level off after a few seconds. The datasets at low (50 and 100 kHz) as well as at high frequencies (500 kHz and 1 MHz) coincide within the error bars. The maximum width of the depletion zone is slightly larger at low frequencies. This reduction of the width might be due to the residual conductivity of the suspension.

It is instructive to compare the data presented above with theoretical considerations. Combining equation (1) with the calculations shown in figure 2 for $\mathrm{d}E^2/\mathrm{d}y$, we can estimate the drift velocity expected for a single colloid subjected to the field gradient. The DEP force on a single colloid is balanced by Stokes friction. In a stationary situation, the velocity is given by the balance of these two forces $v_{\max} = |\vec{v}_{\max}| = (|\vec{F}_{\mathrm{DEP}}|)/(|\vec{F}_{\mathrm{Stokes}}|) = (|\vec{F}_{\mathrm{DEP}}|)/(6\pi r_p \eta)$ (η being the dynamic viscosity of the surrounding medium). Entering the material parameters given above, we find a maximum speed of 2.3 μm s^{-1} at an electric field strength of 1 V μm^{-1}. According to the Stokes–Einstein relation $D = k_{\mathrm{B}}T/6\pi\eta r_p$ (k_{B} being the Boltzmann constant) the diffusion coefficient in our case is 0.2 μm^2 s^{-1}, i.e. it takes a colloid about 1 s to diffuse over a distance of 0.5 μm (radius of one colloid), corresponding to a 'mean velocity' of about 0.5 μm s^{-1}. Consequently, at high field strength, DEP drift dominates colloid motion, especially for long periods and large distances. As the drift velocity is proportional to the square of the field

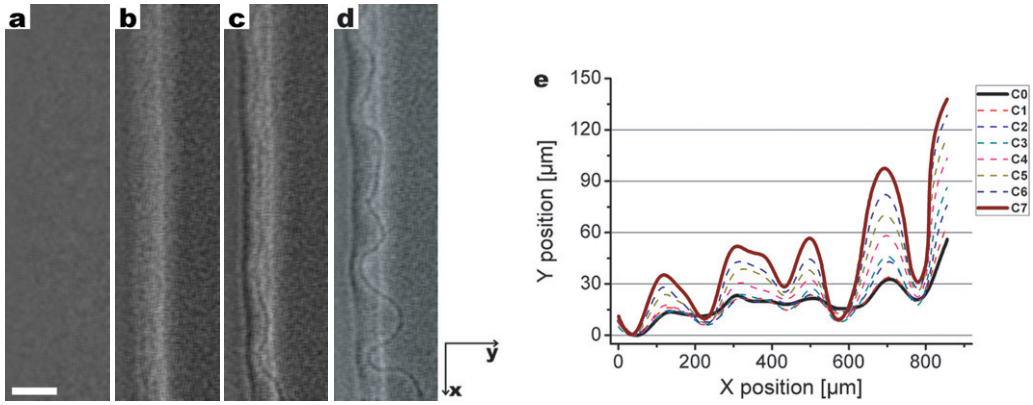

Figure 5. Evolution of the colloid concentration in the gradient region of the electric field. The left side of each image corresponds to the high and the right side to the low field regions. The images were taken (a): 0, (b): 7, (c): 10 and (d): 13 s after turning on the field (1 V μm^{-1}, 100 kHz, sample **B**). Colloid-rich domains appear dark and colloid-depleted ones appear light. The scale bar is 100 μm and the coordinate system is shown at the right of panel (d). (e) The front motion taken from the experiment shown in panels (a)–(d) (relative coordinates with reference to that from the onset time). Curves C0–C7 denote the wavefront position as time moves on. The time between two successive curves is approximately 0.4 s.

strength, a reduction of the field strength by a factor of three reduces the drift velocity by almost one order of magnitude, giving diffusion much more time to compete with DEP drift.

It is important to note that the growth rate of the depletion zone exceeds 20 μm s^{-1} in the highest electric field (see figure 4) and still amounts to a few μm s^{-1} at 0.5 V μm^{-1}. These velocities are significantly above our estimates for the DEP drift velocity. This difference indicates that additional effects play a role in the formation of the depletion zone. As mentioned earlier, the electric field gradient varies over the height of the sample cell. This inhomogeneous field gradient leads to inhomogeneities in the DEP force and might give rise to superimposed hydrodynamic flow.

Thus, balancing the DEP force with Stokes friction explains the different drift velocities of colloids in the gradient region. However, it does not predict the growth rate of the depleted zone.

3.2. Instability of the depletion zone

While the depletion zone is growing, the high field side of the depletion zone develops a darkish rim (see, e.g., figure 3(c)). This indicates a higher concentration of colloids close to the electrode edge. At sufficiently high field strength a wave-like instability develops. Panels (a)–(d) of figure 5 show the temporal evolution of this instability which lasts of the order of 10 s (scale bar 100 μm, field strength 1 V μm^{-1}, frequency 100 kHz). Panel (a) depicts the situation at the moment when the electric field is switched on, i.e. at homogeneous colloid concentration. A few seconds later a depletion zone forms (b) and a rim is visible at the high field side of the depletion zone. After another few seconds the rim develops a wave-like instability (c) which moves across the depletion zone (d). We refer to the time span from turning on the field until the wave pattern first becomes visible as the onset time of the instability.

Figure 5(e) illustrates the front motion observed in the experiment shown in panels (a)–(d). Curves C0–C7 denote the position of the wavefront between 10 and 13 s after turning on the electric field. Since the contour width of the wavefront in the enhanced images (like figures 5(c) and (d)) is about 8 μm, the uncertainty in the front position is a few micrometers. At most positions the front moves along the positive y direction. However, in a few 'valleys' the colloids move opposite to the DEP force. Based on the temporal evolution of the front coordinates, we calculated the velocity as a function of time and position along the x axis. In the observed time interval, the wave amplitude of the front contour is continuously increasing. The velocity of the wavefront is well beyond that of the DEP drift. This strongly supports the hypothesis that this instability is of hydrodynamic origin (see section 4 for further discussion).

To get closer to an understanding of the processes responsible for the observed instability, we analyzed its dependence on various parameters. In a series of experiments at field strengths ranging from 0.5 to 1 V μm^{-1} we calculated the average velocity for each peak of the wavefront over the entire duration of the instability and plotted the maximum wavefront velocity in figure 6(a). It increases almost linearly with field strength. Extrapolating the data towards zero velocity yields a '*critical*' field strength of about 0.3 V μm^{-1}. Indeed, we did not observe any instability at fields below this value.

Figure 6(b) shows that at higher field strengths the instability appears earlier, its duration is shorter and the wave motion is faster. Tests with varying frequencies have shown that neither the timescale nor the maximum wavefront velocity (see figure 6) depend on the applied frequency in a broad range from 50 kHz to 1 MHz. Thus, the slight dependence of the growth rate of the depletion zone on the frequency (see figure 4) has no significant influence on the dynamics of this instability. The existence of a critical field strength can be attributed to the balance between the DEP drift as a driving (destabilizing) force and a combination of viscous friction and diffusion of colloids as a dissipative (stabilizing) mechanism.

We determined the wavelength of the advancing front at electric field strengths ranging from 0.5 to 1 V μm^{-1} by identifying the local minima. The average distance between

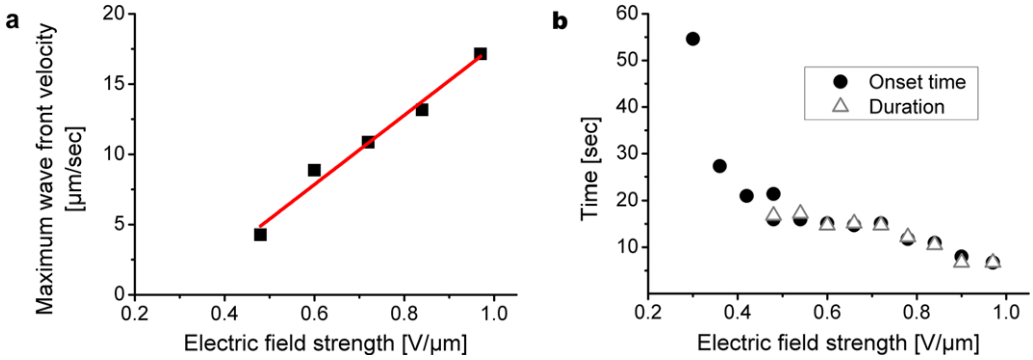

Figure 6. (a) The maximum velocity of peaks of the moving wavefront increases with electric field strength. (b) The onset time (solid circles) and the duration (open triangles) of the instability decrease with field strength. The maximum frame rate of our camera and inaccuracies in identifying the moment when waves first appear lead to an overall uncertainty of about 1 s in determining the onset time and the duration of the instability. Below 0.3 V μm^{-1} no sign of an instability is observed within the first 25 min after turning on the field (sample **B**, frequency 100 kHz).

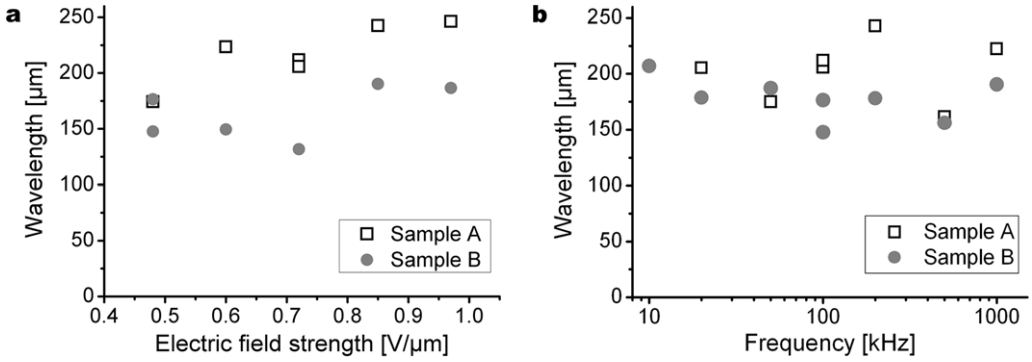

Figure 7. Dependence of the mean wavelength (a) on electric field strength at constant frequency of 100 kHz and (b) on frequency at a constant electric field strength (0.75 V μm^{-1}). The wavelength is independent of the electric field strength. Differences between samples are probably due to variations in sample thickness (see below).

two neighboring minima was taken as the wavelength. In contrast to the results on the average front velocity, the onset time and the duration of the instability, there is no clear dependence of the wavelength on the field strength (see figure 7). The same holds for the frequency dependence. Thus, it is likely the wavelength is not determined by an intrinsic length scale, but dominated by geometrical constraints (e.g. the sample thickness). The measured wavelengths are in the range of the sample thickness and even reflect the slight difference in sample thickness between sample **A** and **B** (see table 2).

4. Ingredients to a modeling of the instability

At various instances in this paper we pointed out that hydrodynamic flow might induce the instability. Certain aspects of this instability resemble the intensively studied Rayleigh–Taylor (RT) instability [25]. In the RT case, a denser fluid is situated above a less dense fluid and gravity acts as a volume force, being higher for denser fluids. The density difference makes the interface between both fluids unstable, leading to the evolution of a finger-like pattern of the denser fluid flowing downward and the less dense fluid flowing upward. The initial stage of the destabilization of the interface is characterized by a spectrum of modes of different wavelength and growth rate [26]. Rayleigh–Taylor instabilities have also been observed in colloidal systems [27].

In our situation the DEP force acting on the single colloids can be regarded as a volume force on length scales large compared to the size of single colloids (e.g. the width of the depletion zone).

Let us exemplify this by discussing the instability of the depletion zone. While the depletion zone is growing, the colloid concentration decreases around the maximum of the field gradient. Once the depletion has formed but is not yet unstable, consider two fluid elements I and II, I being at the maximum of the field gradient and II being in the high field wing of the field gradient. The volume forces on both fluid elements are given by the colloid concentration times the DEP force per colloid. The situation might become unstable, i.e. a hydrodynamic instability can form, if the system can gain energy by exchanging fluid element I with fluid element II. For fluid elements containing colloids the volume force always points towards the low field region and fluid elements free of colloids experience no volume force. In the extreme case of a vanishing colloid concentration at the maximum of the field gradient the volume force on element I tends towards zero while the volume force on element II is still finite. Thus moving element I to the position of II costs no energy, whereas

energy is gained by moving element II to the position of I. This situation resembles those required for the Rayleigh–Taylor instability. Therefore the interface can become unstable and a hydrodynamic flow can develop. The energetic argument we used here is a necessary condition for instability. Due to the presence of dissipative (stabilizing) mechanisms like diffusion or viscosity, the onset of the instability can be influenced, leading to a critical driving force. But this does not alter the possibility for an instability.

However, in comparison to Rayleigh–Taylor, the instability near the edges of an electric bottle cannot be mapped directly onto an RT instability. For standard RT instability the volume force is laterally constant as long as the system is stable. In our case the electric field strength varies across the sample height. This essentially makes the situation more complex and prohibits a direct comparison. The bulk analysis of the RT instability [26] predicts a dependence of the wavelength on the density difference. In our case this would imply a dependence of the wavelength on the applied electric field, which was not observed.

5. Conclusion

We investigated the motion of PMMA colloids in a density-matching mixture of CHB and *trans*-decalin in a non-uniform alternating electric field.

Due to the field gradient at the electrode edge, the colloids were driven out of the electric bottle. Since the DEP force is inhomogeneous within the field gradient region, a zone depleted of colloids developed around the local maximum of the DEP force. The time required for formation and growth of the depletion zone decreased with increasing field gradient. Furthermore, we observed the formation of a colloid-rich rim at the high field side of the depletion zone that exhibited a wave-like instability at sufficiently high field strengths. While the instability occurred and disappeared faster at higher field strength, it was independent of frequency. Its wavelength seems to depend on geometrical constraints such as sample thickness. We have argued that the instability results from the interplay of the DEP force on colloids on the one hand and the volume force on the solvent caused by colloid migration on the other. The basic driving force of the observed instability (an inversion of the volume force density) is comparable to the RT instability.

Acknowledgments

It is a pleasure for the authors to thank Hartmut Löwen and Adam Wysocki for interesting and stimulating discussions and Beate Ullrich for carefully reading the manuscript. This work has been financially supported by the DFG through the SFB TR6.

References

[1] Pohl H A 1958 Some effects of nonuniform fields on dielectrics *J. Appl. Phys.* **29** 1182–8
[2] Kang Y J, Li D Q, Kalams S A and Eid J E 2008 Dc-dielectrophoretic separation of biological cells by size *Biomed. Microdevices* **10** 243–9
[3] van Blaaderen A 1998 Materials science-opals in a new light *Science* **282** 887–8
[4] van Blaaderen A 2003 Colloidal molecules and beyond *Science* **301** 470–1
[5] Applegate R W, Squier J, Vestad T, Oakey J and Marr D W M 2004 Optical trapping, manipulation, and sorting of cells and colloids in microfluidic systems with diode laser bars *Opt. Express* **12** 4390–8
[6] Chang C C and Yang R J 2007 Electrokinetic mixing in microfluidic systems *Microfluid. Nanofluid.* **3** 501–25
[7] Vossen D L J, Fific D, Penninkhof J, van Dillen T, Polman A and van Blaaderen A 2005 Combined optical tweezers/ion beam technique to tune colloidal masks for nanolithography *Nano Lett.* **5** 1175–9
[8] Urdaneta M and Smela E 2007 Multiple frequency dielectrophoresis *Electrophoresis* **28** 3145–55
[9] Gascoyne P R C and Vykoukal J 2002 Particle separation by dielectrophoresis *Electrophoresis* **23** 1973–83
[10] van Blaaderen A 2004 Colloids under external control *MRS Bull.* **29** 85–90
[11] Jia B P and Gao L 2008 Morphological transformation of Fe_3O_4 spherical aggregates from solid to hollow and their self-assembly under an external magnetic field *J. Phys. Chem.* C **112** 666–71
[12] Zheng L F, Li S D, Brody J P and Burke P J 2004 Manipulating nanoparticles in solution with electrically contacted nanotubes using dielectrophoresis *Langmuir* **20** 8612–9
[13] Zhou H, White L R and Tilton R D 2005 Lateral separation of colloids or cells by dielectrophoresis augmented by ac electroosmosis *J. Colloid Interface Sci.* **285** 179–91
[14] Pohl H A and Hawk I 1966 Separation of living and dead cells by dielectrophoresis *Science* **152** 647–9
[15] Deval J, Tabeling P and Ho C-M 2002 A dielectrophoretic chaotic mixer *15th IEEE Int. Conf. on Micro Electro Mechanical Systems 2002* ed P Tabeling, pp 36–9
[16] Vossen D L J, Plaisier M A and van Blaaderen A 2004 Colloidal crystallization induced by optical gradient forces exerted by optical tweezers *Proc. SPIE* **5514** 755–62
[17] Sullivan M, Zhao K, Harrison C, Austin R H, Megens M, Hollingsworth A, Russel William B, Cheng Z, Mason T and Chainkin P C 2003 Control of colloids with gravity, temperature gradients and electric fields *J. Phys.: Condens. Matter* **15** S11–8
[18] Sullivan M T, Zhao K, Hollingsworth A D, Austin R H, Russel W B and Chaikin P M 2006 An electric bottle for colloids *Phys. Rev. Lett.* **96** 015703
[19] Leunissen M E, Sullivan M T, Chaikin P M and van Blaaderen A 2008 Concentrating colloids with electric field gradients. I. Particle transport and growth mechanism of hard-sphere-like crystals in an electric bottle *J. Chem. Phys.* **128** 164508
[20] Leunissen M E and van Blaaderen A 2008 Concentrating colloids with electric field gradients. II. Phase transitions and crystal buckling of long-ranged repulsive charged spheres in an electric bottle *J. Chem. Phys.* **128** 164509
[21] Jones T B 1995 *Electromechanics of Particles* (Cambridge: Cambridge University Press)
[22] Antl L, Goodwin J W, Hill R D, Ottewill R H, Owens S M, Papworth S and Waters J A 1986 The preparation of poly(methyl methacrylate) lattices in nonaqueous media *Colloids Surf.* **17** 67–78
[23] Leunissen M E 2007 Manipulating colloids with charges and electric fields *PhD Thesis* Utrecht University http://www.colloid.nl/Theses/Leunissen_Thesis_2007.pdf

[24] http://femm.foster-miller.net/wiki/HomePage
[25] Rayleigh L 1882 Investigation of the character of the equilibrium of an incompressible heavy fluid of variable density *Proc. London Math. Soc.* **s1-14** 170–7
[26] Chandrasekhar S 1961 *Hydrodynamic and Hydromagnetic Stability* (New York: Oxford University Press)
[27] Völtz C, Pesch W and Rehberg I 2001 Rayleigh–Taylor instability in a sedimenting suspension *Phys. Rev.* E **65** 011404